

Supporting Information
for
**Stabilized open metal sites in bimetallic metal–organic framework catalysts for hydrogen
production from alcohols**

Jonathan L. Snider,^a Ji Su,^b Pragya Verma,^c Farid El Gabaly,^a Joshua D. Sugar,^a Luning Chen,^b Jeffery M. Chames,^a A. Alec Talin,^a
Chaochao Dun,^c Jeffrey J. Urban,^c Vitalie Stavila,^a David Prendergast,^c Gabor A. Somorjai,^{bd} and Mark D. Allendorf^{*a}

-
- ^{a.} *Sandia National Laboratories*
7011 East Ave MS 9161, Livermore, CA, 94550, USA
- ^{b.} *Materials Sciences Division, Lawrence Berkeley National Laboratory*
Building 66, One Cyclotron Road, Berkeley, CA 94720, USA
- ^{c.} *Molecular Foundry, Lawrence Berkeley National Laboratory*
Building 67, One Cyclotron Road, Berkeley, CA, 94720, USA
- ^{d.} *Department of Chemistry, University of California – Berkeley*
D56 Hildebrand Hall, Berkeley, CA, 94720, USA
- * Corresponding author, e-mail: mdallen@sandia.gov

Table of Contents

Item	Description	Page No.
Section S1	Additional experimental methods	3
Figure S1	N ₂ adsorption-desorption isotherms of M-MOF-74	4
Table S1	Nearest metal-metal distances of M-MOF-74 before and after adsorption	4
Figure S2	Appearance of Ni-MOF-74 as prepared and after testing at 300 °C	4
Figure S3	Raman spectroscopy of MOF-74 catalysts before and after testing	5
Figure S4	Characterization of Ni-MOF-74 after catalysis at 300 °C	5
Figure S5	Stability of Ni-MOF-74 under methanol dehydrogenation conditions	6
Table S2	Elemental composition of the (Ni _x Mg _{1-x})-MOF-74 catalyst series	6
Section S2	Discussion of elemental analysis results: SEM-EDS & ICP-OES	7
Figure S6	N ₂ adsorption-desorption isotherms of (Ni _x Mg _{1-x})-MOF-74 catalyst	8
Figure S7	Normalized Mg 1s XPS spectra of the (Ni _{0.32} Mg _{0.68})-MOF-74 catalyst	8
Figure S8	Characterization of (Ni _{0.32} Mg _{0.68})-MOF-74 after catalysis at 300 °C	9
Figure S9	XPS of (Ni _{0.32} Mg _{0.68})-MOF-74 after 24 hours of catalysis at 250 °C	9
Table S3	TOF of methanol dehydrogenation catalysts	10
Figure S10	Catalytic performance of dried Raney Ni catalyst	10
Figure S11	Model structures for DFT calculations	11
Table S4	Comparison between cluster and periodic models	12
Table S5	Adsorption energies of methanol in M-MOF-74	12
Table S6	Adsorption energies of carbon monoxide in M-MOF-74	12
Figure S12	Geometry of M-MOF-74 transition state structures	13-14
Figure S13	Geometry of Ni-MOF-74 transition state structures	15
Table S7	Barrier heights and reaction energies for M-MOF-74 catalysts	15
Figure S14	Reduced barriers with linker assistance	16
Table S8	Lattice parameters and volumes of bimetallic MOF-74 structures	16
Figure S15	Structures of six bimetallic (Ni _x Mg _{1-x})-MOF-74 systems	17
Figure S16	Dependence of methanol conversion on feed rate	17
References		18

Section S1. Additional experimental methods

Mg-MOF-74 synthesis: A similar procedure to that of the bimetallic MOF was utilized. In a 250 mL glass bottle, 80 mL DMF, 4 mL ethanol, and 4 mL deionized water were mixed. To this, 0.198 g (1 mmol) of 2,5-dihydroxyterephthalic acid and 0.729 g (2.8 mmol) of magnesium(II) nitrate hexahydrate were dissolved by sonication. Heating and washing steps followed as described for the bimetallic MOF. Mg-MOF-74 was also prepared from magnesium(II) chloride and found to be similarly inactive for catalysis.

Ni-MOF-74 synthesis: A similar procedure to that of the bimetallic MOF was utilized. In a 250 mL glass bottle, 160 mL DMF, 8 mL ethanol, and 8 mL deionized water were mixed. To this, 0.41 g (2.1 mmol) of 2,5-dihydroxyterephthalic acid and 1.82 g (6.3 mmol) of nickel(II) nitrate hexahydrate were dissolved by sonication. Heating and washing steps followed as described for the bimetallic MOF. Ni-MOF-74 was also prepared from nickel(II) chloride and found to have similar performance.

Co-MOF-74 synthesis: A similar procedure to that of the bimetallic MOF was utilized. In a 250 mL glass bottle, 160 mL DMF, 8 mL ethanol, and 8 mL deionized water were mixed. To this, 0.41 g (2.1 mmol) of 2,5-dihydroxyterephthalic acid and 1.81 g (6.3 mmol) of cobalt(II) nitrate hexahydrate were dissolved by sonication. Heating and washing steps followed as described for the bimetallic MOF.

Mn-MOF-74 synthesis: A similar procedure to that of the bimetallic MOF was utilized. In a 250 mL glass bottle, 160 mL DMF, 8 mL ethanol, and 8 mL deionized water were mixed. To this, 0.41 g (2.1 mmol) of 2,5-dihydroxyterephthalic acid and 1.58 g (6.3 mmol) of manganese(II) nitrate tetrahydrate were dissolved by sonication. Heating and washing steps followed as described for the bimetallic MOF.

Cu-MOF-74 synthesis: The Cu-MOF-74 synthesis was adapted from literature.⁵ In a 250 mL glass bottle, 60 mL DMF, and 2 mL 2-propanol were mixed. To this, 0.55 g (2.8 mmol) of 2,5-dihydroxyterephthalic acid and 1.48 g (6.1 mmol) of copper(II) nitrate trihydrate were dissolved by sonication. The solution was capped and heated at 80 °C for 16 hours. Washing steps followed as described for the bimetallic MOF.

Raman spectroscopy: Raman spectra were collected using a Renishaw InVia confocal Raman microscope with a 532 nm excitation wavelength and power at the sample of <0.2 mW to avoid excessive heating.

Inductively coupled plasma-optical emission spectrometry (ICP-OES): Samples were analyzed on a Varian ICP-OES 720 Series to determine an accurate loading of Mg and Ni. MOF-74 samples (~0.05 mmol) was fully dissolved in 1 mL Aqua regia (2 days), and then diluted in 4 mL of 2 wt% HNO₃. 2.5 mL of the solvent was taken and further diluted with 6.5 mL of 2 wt% HNO₃. 1000 ppm Magnesium and Nickel standard solutions (Sigma Aldrich) were used to prepare diluted standard solutions having Mg/Ni concentrations ranging from 5 to 100 ppm.

Metrics for catalytic performance: Catalyst performance was calculated using the following equations:

$$H_2 \text{ Productivity} \left(\frac{\text{ml}}{\text{g}_{\text{cat}} \cdot \text{min}} \right) = \frac{H_2 \text{ Production Volume (ml) at 1 atm and 25 }^\circ\text{C}}{\text{Mass catalyst (g)} \times \text{Time (min)}} \quad \text{Equation 1}$$

$$\text{Methanol Conversion (\%)} = \frac{H_2 \text{ Production Rate} \left(\frac{\text{mol}}{\text{min}} \right)}{2 \times \text{Methanol Feeding Rate} \left(\frac{\text{mol}}{\text{min}} \right)} \times 100\% \quad \text{Equation 2}$$

$$\text{Carbon Selectivity towards X (\%)} = \frac{m_X C_X}{\sum_i m_i C_i} \times 100\% \quad \text{Equation 3}$$

$$\text{Turnover Frequency (TOF) (hr}^{-1}\text{)} = \frac{\text{Methanol consumption rate} \left(\frac{\text{mol}}{\text{hr}} \right)}{\text{Moles of Ni}} \quad \text{Equation 4}$$

where 'm' is the moles of a given product produced and 'C' is the number of carbon atoms in a formula unit of X.

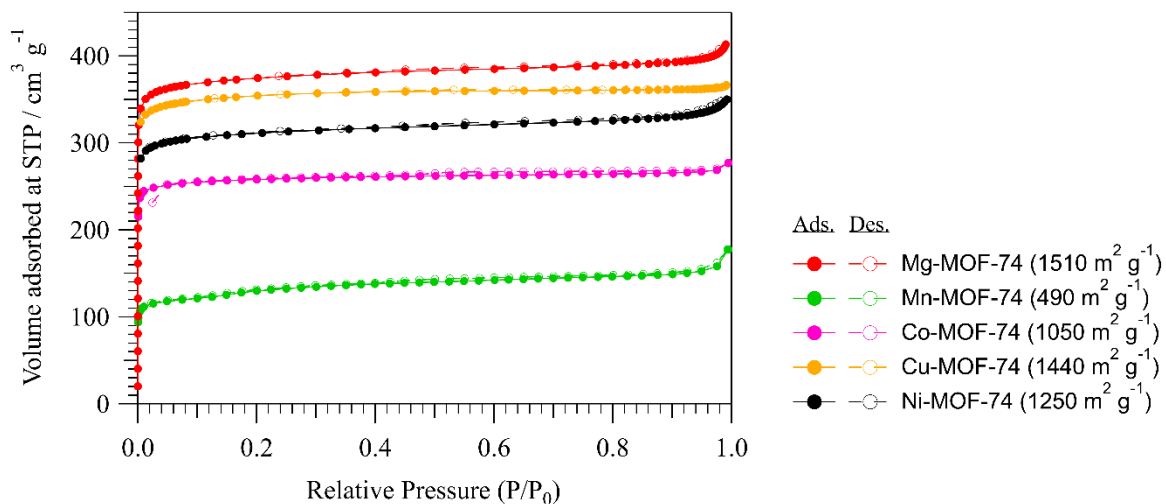


Figure S1. N₂ adsorption-desorption isotherms of M-MOF-74 catalyst series collected at 77 K.

Table S1. Nearest metal-metal (M–M) distances calculated for the M-MOF-74 series before and after adsorption of methanol using the periodic model. Calculations performed using rev-vdW-DF2 for Mg-MOF-74 and Zn-MOF-74 and using rev-vdW-DF2+U for Mn-MOF-74, Co-MOF-74, Ni-MOF-74, and Cu-MOF-74.

Metal in M-MOF-74	U^a	M–M distance before adsorption (Å)	M–M distance after adsorption (Å)
Cu	4.0	2.97	3.12
Co	3.3	2.92	2.99
Mg	-	2.92	3.01
Mn	4.0	3.08	3.17
Ni	6.4	2.86	2.95
Zn	-	2.93	3.05

^aNo U correction was applied to Mg and Zn.



Figure S2. Visual appearance of (left) Ni-MOF-74 as prepared and (right) Ni-MOF-74 after testing at 300 °C. The catalyst presented after testing is still mixed with clear glass beads.

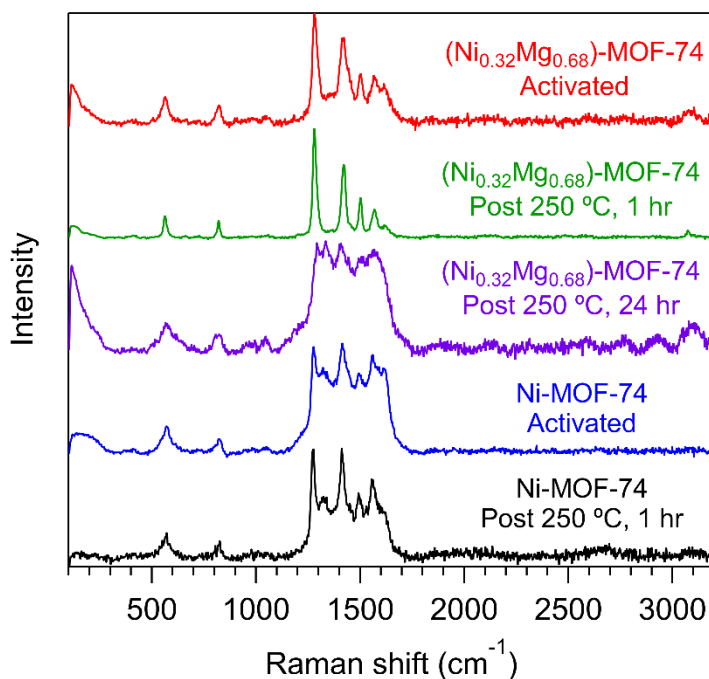


Figure S3. Raman spectroscopy of MOF-74 catalysts before and after catalysis at 250 °C. The sharp, distinct peaks of the MOF-74 structure are visible in the $(\text{Ni}_{0.32}\text{Mg}_{0.68})\text{-MOF-74}$ sample, both as activated and after 1 hour of catalysis, suggesting that the uniform structure of the framework is maintained. A significant broadening of the peaks is observed after 24 hours of catalysis, consistent with the broad Raman feature of amorphous carbon.² Broad features are also observed for the Ni-MOF-74 catalyst after 1 hour of catalysis, indicating again the presence of amorphous carbon (as suggested by Figure 3d). Interestingly, broad peaks are also observed in the activated Ni-MOF-74, suggesting that the framework can degrade during activation, as reported previously.⁴

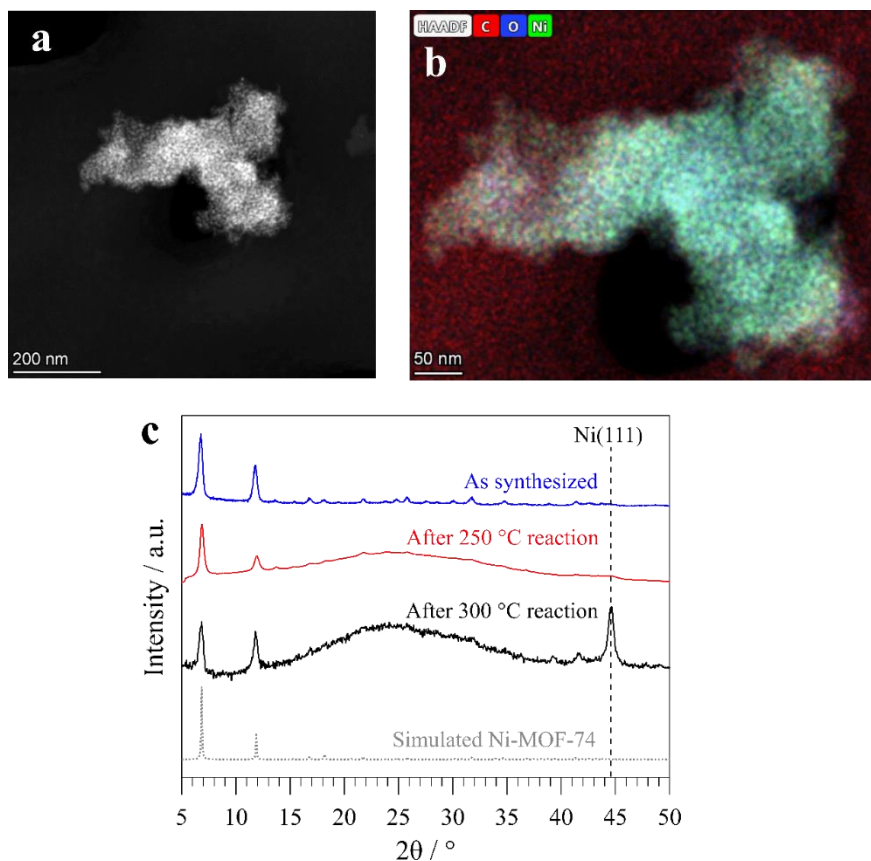


Figure S4. Characterization of Ni-MOF-74 before and after performing methanol dehydrogenation for 1 hour at 300 °C and 1 atm. (a) Dark field TEM image and (b) TEM-EDS maps of a large Ni agglomerate observed after catalytic testing. (c) XRD patterns of the catalyst before and after testing, compared to a simulated Ni-MOF-74 reference (CSD-LECQEQ).³

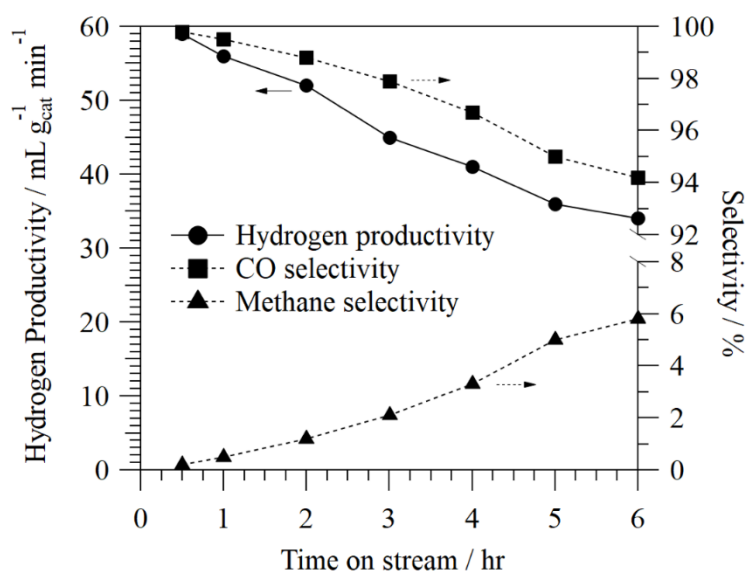


Figure S5. Stability of Ni-MOF-74 under methanol dehydrogenation conditions (0.1 mL min⁻¹ methanol, 35 sccm N₂, 100 mg Ni-MOF-74, 1 atm, 250 °C).

Table S2. Elemental composition of the (Ni_xMg_{1-x})-MOF-74 catalyst series. The Ni metal fraction in the final product is found to be greater than the molar fraction of Ni in the metal salts used in the synthesis. Elemental compositions (at %) determined by SEM-EDS for powders pressed into indium foil and averaged across three regions of each sample. Metal composition was also analyzed by ICP-OES. The amount of metal (mmol) present in the 10-15 mg samples is shown. See Section S2 below for a discussion of the elemental analysis.

Sample, M (M-MOF-74)	Ni metal fraction, x in (Ni _x Mg _{1-x})			Product Composition via SEM-EDS (at%)				Metal content via ICP-OES		
	Synthesis mixture	Product via SEM-EDS	Product via ICP-OES	Ni	Mg	C	O	Sample mass (mg)	Ni (mmol)	Mg (mmol)
Mg	0	0	0	0.0	11.4	48.8	39.0	10.0	0	55.6
(Ni _{0.01} Mg _{0.99})	0.01	0.01	0.01	0.1	11.5	47.0	41.3	12.6	0.8	63.5
(Ni _{0.17} Mg _{0.83})	0.1	0.17	0.14	2.1	10.6	48.7	38.5	14.0	6.3	40.2
(Ni _{0.32} Mg _{0.68})	0.2	0.32	0.27	3.7	8.0	51.0	37.1	14.4	14.4	38.7
(Ni _{0.54} Mg _{0.46})	0.4	0.54	0.48	7.0	5.9	49.1	37.9	13.8	27.3	28.4
(Ni _{0.76} Mg _{0.24})	0.6	0.76	0.75	9.0	2.9	49.8	38.2	14.0	31.4	10.6
Ni	1	1	1	16.9	0	49.6	33.2	10.0	28.0	0

Section S2. Discussion of elemental analysis

The elemental analysis is consistent with the theoretical structure of $M_2(\text{dobdc})$ and supports the assignment of the metal species to framework positions. First, SEM-EDS was performed on samples that were heated under vacuum to remove adsorbed water. Regions of the sample with sufficient MOF thickness to mask the signal from the underlying indium foil were selected, and the result was averaged over three such regions. EDS data was collected for nickel, magnesium, carbon, and oxygen. Looking at these four elements, we observe consistent trends in the bimetallic sample compositions. On average, the composition was 12.2 at% total metal (Ni+Mg), 49.1 at% carbon, and 38.6 at% oxygen. These values agree well with the theoretical formula for MOF-74: $M_2C_8H_2O_6$. Recognizing that SEM-EDS cannot detect hydrogen, the adjusted formula of " $M_2C_8O_6$ " gives a composition of 12.5 at% metal, 50 at% carbon, and 37.5 at% oxygen. This excellent agreement confirms the $M_2(\text{dobdc})$ stoichiometry in the bimetallic samples and indicates that the metals are in framework positions. The one exception is the monometallic Ni-MOF-74 sample which shows an excess of Ni and may indicate some decomposition during activation or non-framework nickel contamination in this sample.

Next, ICP-OES analysis was performed to confirm the compositions. Samples for ICP-OES had been stored in air and were not activated prior to analysis. As such, the frameworks will have some degree of water (or other guest molecule) saturation and the true mass of the guest-free MOF is unknown. For example, the Mg-MOF-74 sample gives a stoichiometry of 1.3:1 Mg:linker if we assume the material is fully activated (242.6 g mol^{-1}). If the sample is instead assumed to be saturated with $\sim 0.4 \text{ g H}_2\text{O/g MOF}$ (339.6 g mol^{-1}),⁶ then we get a result of 1.9:1 Mg:linker. Again, this agrees well with the $M_2(\text{dobdc})$ stoichiometry and suggests the metals in this sample are in framework positions. However, we are unable to reliably apply this same analysis to all the samples as they've experienced different storage conditions and the degree of air exposure and MOF saturation are unknown.

As shown in Table 2, the sample series has an apparent metal deficiency via ICP-OES. Given the unknown MOF saturation, as well as the possibility of undissolved metals after sample digestion, the absolute metal loading from ICP-OES has a large degree of uncertainty. However, the Ni:Mg ratio can be determined without knowing the true molecular weight of the sample. These values, shown in Table S2, agree well with the results obtained via SEM-EDS, giving further confidence that the probe depth of SEM-EDS, on the order of a micron, is not skewing the results.

Due to the uncertainty described above, we have chosen to identify and normalize the samples by the SEM-EDS results. We believe the SEM-EDS results will be more accurate for the TOF calculations because (1) the samples were in an activated state prior to measurement, (2) the results agree with the theoretical composition, and (3) the metal ratios agree well with ICP-OES giving us confidence that the measurement is accurate. Furthermore, selecting the SEM-EDS results is the more conservative approach as this shows larger nickel loadings than the ICP-OES results. If the ICP-OES results are more representative, than the TOFs shown in Table S3 are underestimates of the catalyst's true activity.

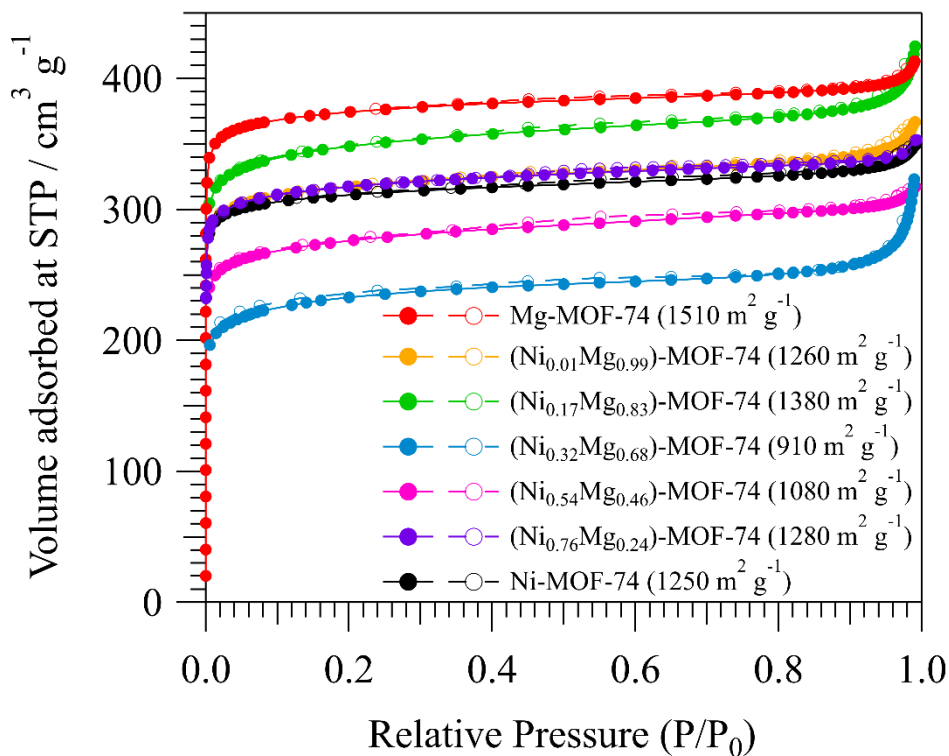


Figure S6. N_2 adsorption-desorption isotherms of the (Ni_xMg_{1-x}) -MOF-74 catalyst series collected at 77 K. Filled symbols trace the adsorption isotherm while open symbols trace the desorption isotherm. Multi-point BET surface areas shown in parenthesis.

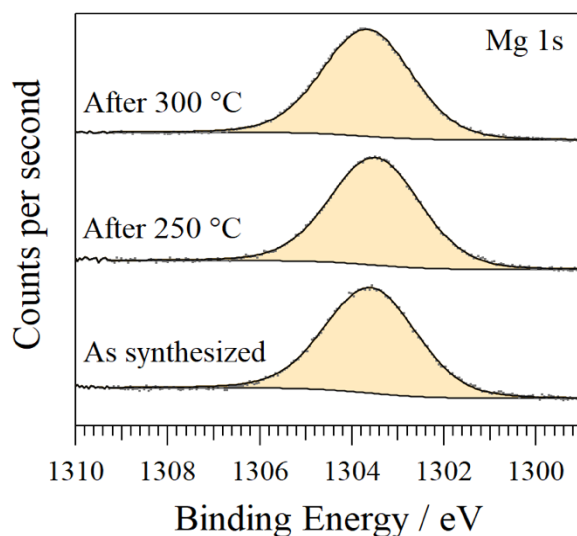


Figure S7. Normalized Mg 1s XPS spectra of the $(Ni_{0.32}Mg_{0.68})$ -MOF-74 catalyst: as synthesized, after 1 hour of methanol dehydrogenation at 250 °C, and after 1 hour of methanol dehydrogenation at 300 °C. Experimental data (grey points) fit with a single peak for the Mg^{2+} OMS in the MOF.

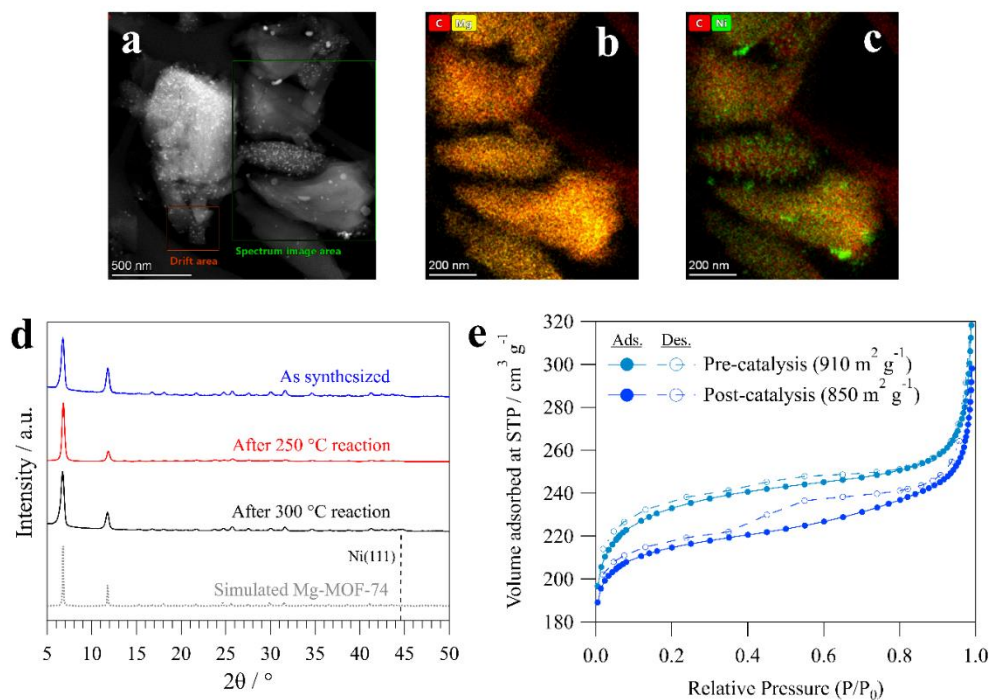


Figure S8. Characterization of $(\text{Ni}_{0.32}\text{Mg}_{0.68})\text{-MOF-74}$ before and after performing methanol dehydrogenation for 1 hour at 300 °C and 1 atm. (a) Dark field TEM image and (b, c) TEM-EDS maps of the catalyst after testing. (d) XRD patterns of the catalyst before and after testing, compared to a simulated Mg-MOF-74 reference (CSD-VOGTIV).¹ (e) N_2 isotherms and BET surface area of catalyst collected at 77 K before and after catalytic testing.

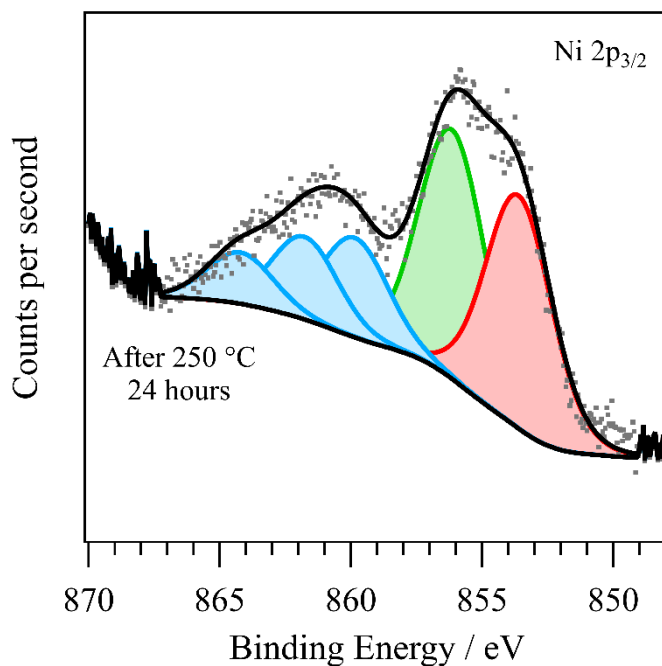


Figure S9. Normalized Ni $2p_{3/2}$ XPS spectra of $(\text{Ni}_{0.32}\text{Mg}_{0.68})\text{-MOF-74}$ after testing at 250 °C for 24 hours. Experimental data (grey points) fit with a Ni^0 peak (red), Ni^{2+} peak (green), and several satellite peaks (blue) to create the envelope shown (black line).

Table S3. Weight hourly space velocity (WHSV), turnover frequencies (TOF), and active material loading of several methanol dehydrogenation catalysts reported in the literature. TOFs are calculated based on the moles of methanol consumed. Values for Ni-MOF-74 and (Ni_{0.32}Mg_{0.68})-MOF-74 are normalized based on the SEM-EDS results. Values for Co-MOF-74 are estimated based on the theoretical structure, as elemental analysis of this sample was unavailable. TOF values for Raney Ni are a range based on the manufacturer's specification for nickel.

Material	Temperature (°C)	WHSV (g _{MeOH} g ⁻¹ _{catalyst} hr ⁻¹)	TOF (hr ⁻¹)	Active metal loading (wt%)	Reference
(Ni _{0.32} Mg _{0.68})-MOF-74	250	47.5	31.4	13.5	This work
(Ni _{0.32} Mg _{0.68})-MOF-74	300	47.5	105	13.5	This work
Ni-MOF-74	300	47.5	24	47	This work
Co-MOF-74	300	47.5	22 (est.)	37.8 (est.)	This work
Raney Ni	250	105.6	36.5-41	89-100	This work
Raney Ni	300	105.6	86.5-97.2	89-100	This work
Ni/BN	300	23.8	238	10	7
Ni-1/SiO ₂	238	0.75	11	3.63	8
Pd/CeO ₂	200	2	94	15	9
Pt ₁ /CeO ₂	300	47.5	12,500	0.15	10
Ni/SiO ₂	200	-	4.3	1	11
Rh/SiO ₂	200	-	11	1	11
Pt/SiO ₂	200	-	40	1	11
Pd/SiO ₂	200	-	137	1	11

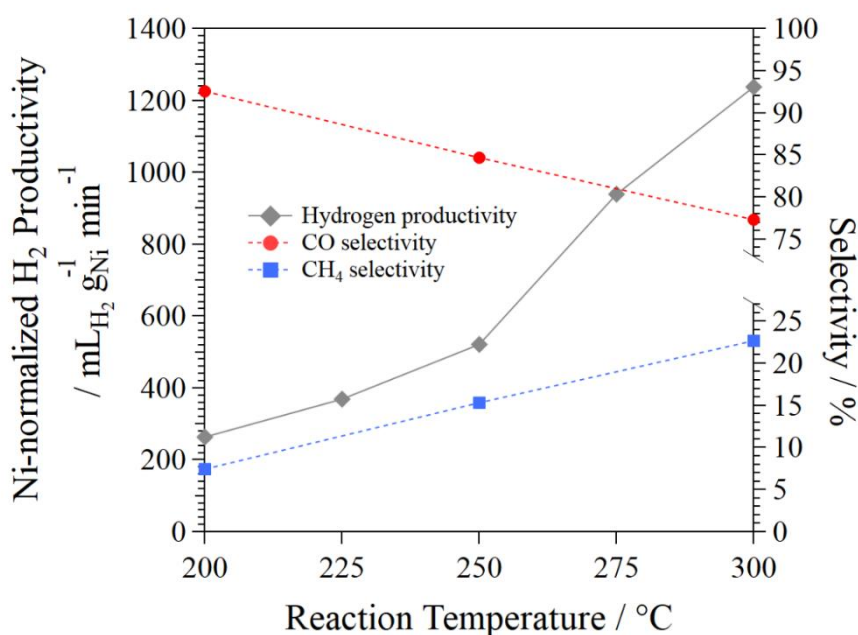


Figure S10. Catalytic performance of dried Raney Ni catalyst towards methanol dehydrogenation: nickel-normalized hydrogen productivity (grey diamonds) and product selectivity towards CO (red circles) and CH₄ (blue squares). Reaction conditions: 0.1 mL min⁻¹ methanol, 35 sccm N₂, 45 mg catalyst, 1 atm.

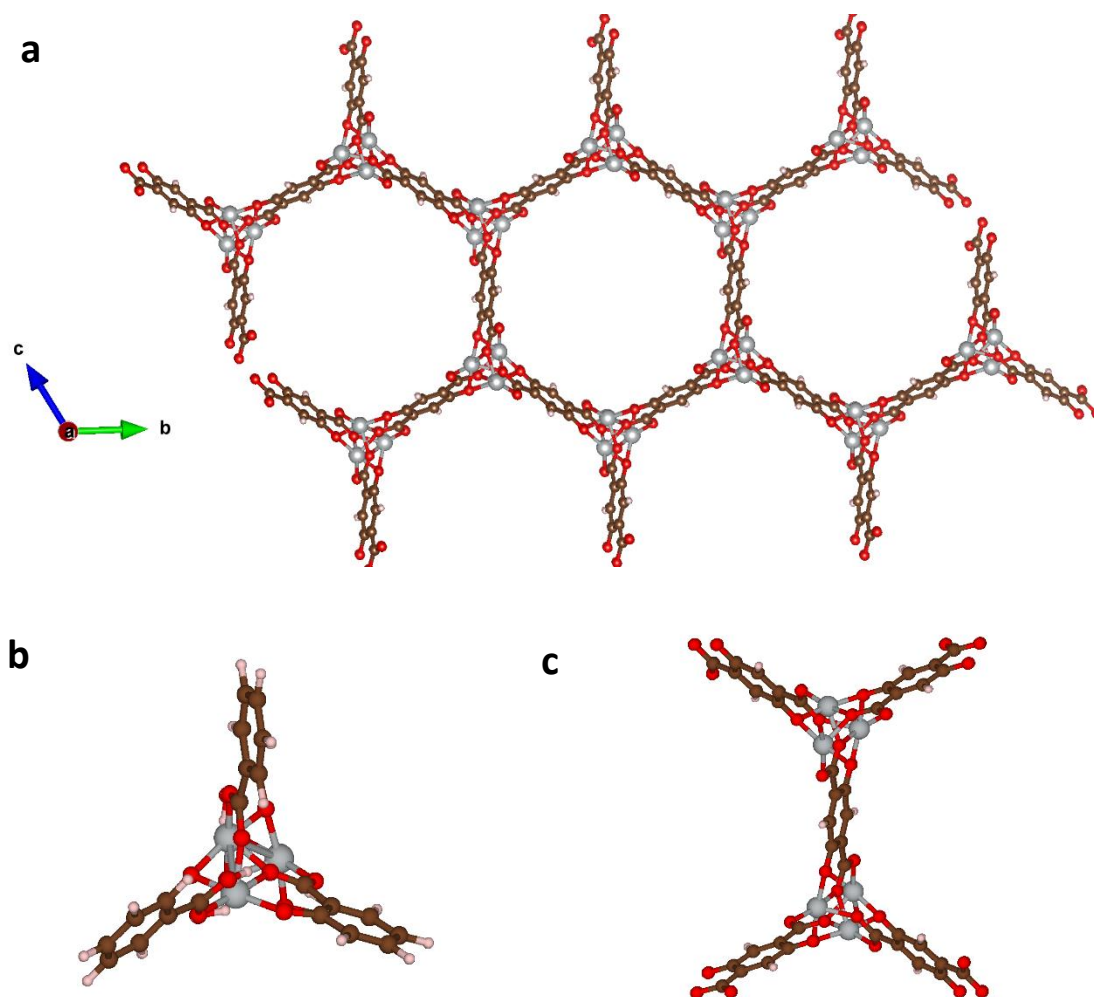


Figure S11. Ball-and-stick models of structures used in the computational investigation of M-MOF-74: (a) extended chemical structure, (b) unit cell used to construct the periodic model, (c) 88-atom cluster model (Color coded such that metal = gray, oxygen = red, carbon = black, hydrogen = white).

Table S4. Comparison between cluster and periodic models for key bond distances and binding energies^a calculated by the PBE functional for Mg-MOF-74 and Ni-MOF-74 bound to H₂, CO, HCHO, and CH₃OH. Experimental isosteric heats of adsorption (Q_{st}) included as additional validation of the models.

MOF	Adsorbate	Cluster Model		Periodic Model		Q_{st} (kcal mol ⁻¹)
		ΔE (kcal mol ⁻¹)	M–A (Å) ^b	ΔE (kcal mol ⁻¹)	M–A (Å) ^b	
Mg-MOF-74	H ₂	-1.8	2.50	-1.8	2.46	-2.7 ¹²
	CO	-7.1	2.48	-6.2	2.48	-6.9 ¹³
	HCHO	-11	2.20	-11.9	2.16	-
	CH ₃ OH	-17.1	2.18	-14.5	2.16	-
Ni-MOF-74	H ₂	-2.5	2.04	-2.1	1.97	-3.1 ¹⁴
	CO	-15.8	1.92	-15.9	1.88	-
	HCHO	-8.9	2.13	-9.5	2.08	-
	CH ₃ OH	-12.8	2.18	-11.4	2.17	-

^aBinding energy = energy of the complex – energy of the monomers.

^bM–A is the metal adsorbate distance.

Table S5. Adsorption energies (ΔE)^a of methanol in M-MOF-74 calculated using the rev-vdW-DF2+U method with the periodic model.

Metal in M-MOF-74	U^b	ΔE_{MeOH} (kcal mol ⁻¹)
Cu	4.0	-11.6
Co	3.3	-18.3
Mg	-	-21.7
Mn	4.0	-16.7
Ni	6.4	-19.2
Zn	-	-17.1

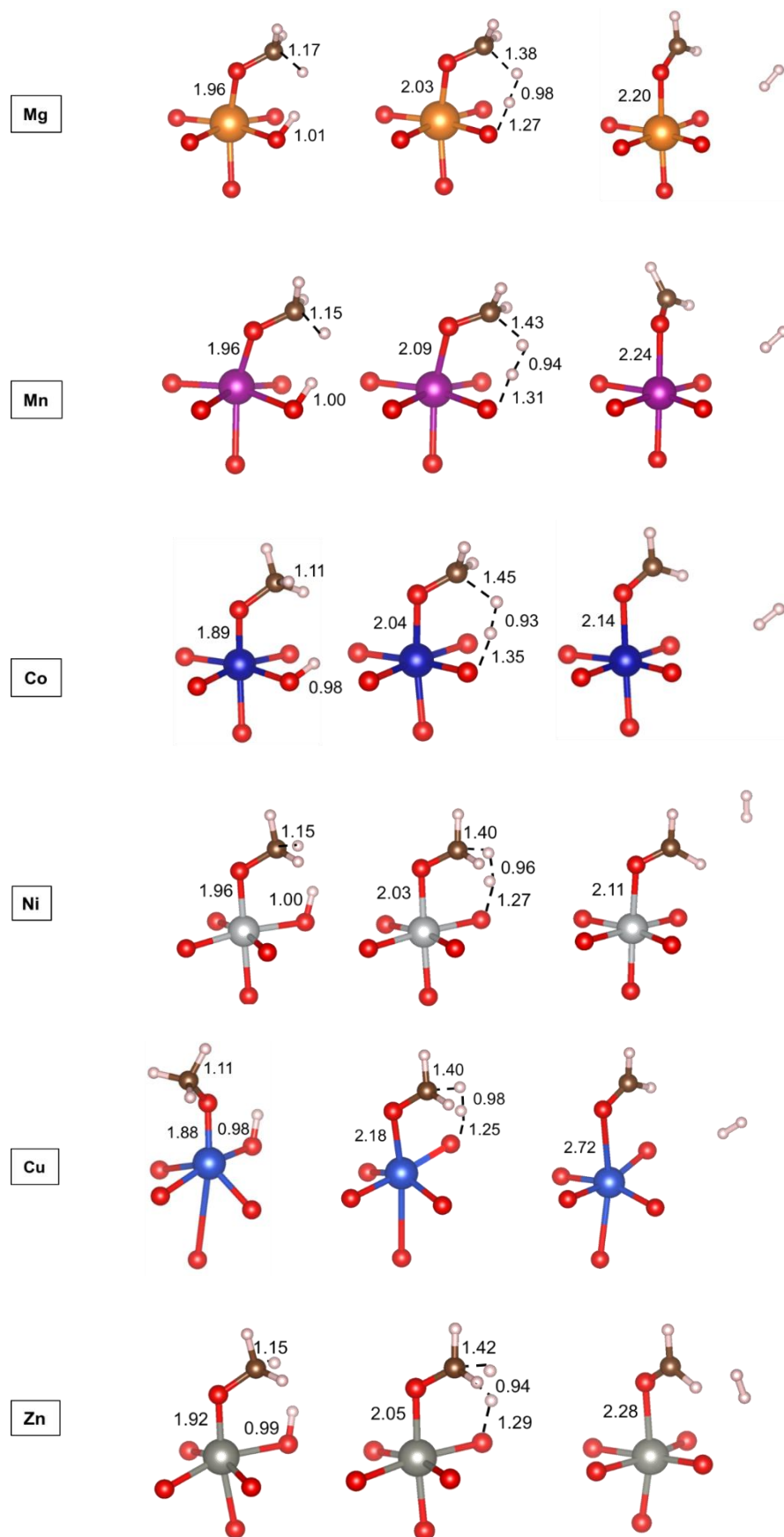
^aAdsorption energy = energy of the complex – energy of the monomers.

^bNo +U correction was applied to Mg and Zn.

Table S6. Binding energies (ΔE)^a of carbon monoxide in M-MOF-74 calculated by PBE/def2-TZVP for binding via carbon (CO) and via oxygen (OC) ends. All calculations are performed with the 88-atom cluster model at 0 K.

Metal in M-MOF-74	ΔE_{CO} (kcal mol ⁻¹)	ΔE_{OC} (kcal mol ⁻¹)
Cu	-0.0	-0.0
Co	-18.8	-1.2
Mg	-7.1	-2.6
Mn	-7.2	-1.3
Ni	-15.8	-1.4
Zn	-5.6	-1.4

^aBinding energy = energy of the complex – energy of the monomers.

(a) Transition structure for Reaction 1 and the intermediates around it

(b) Transition structure for Reaction 2 and the intermediates around it

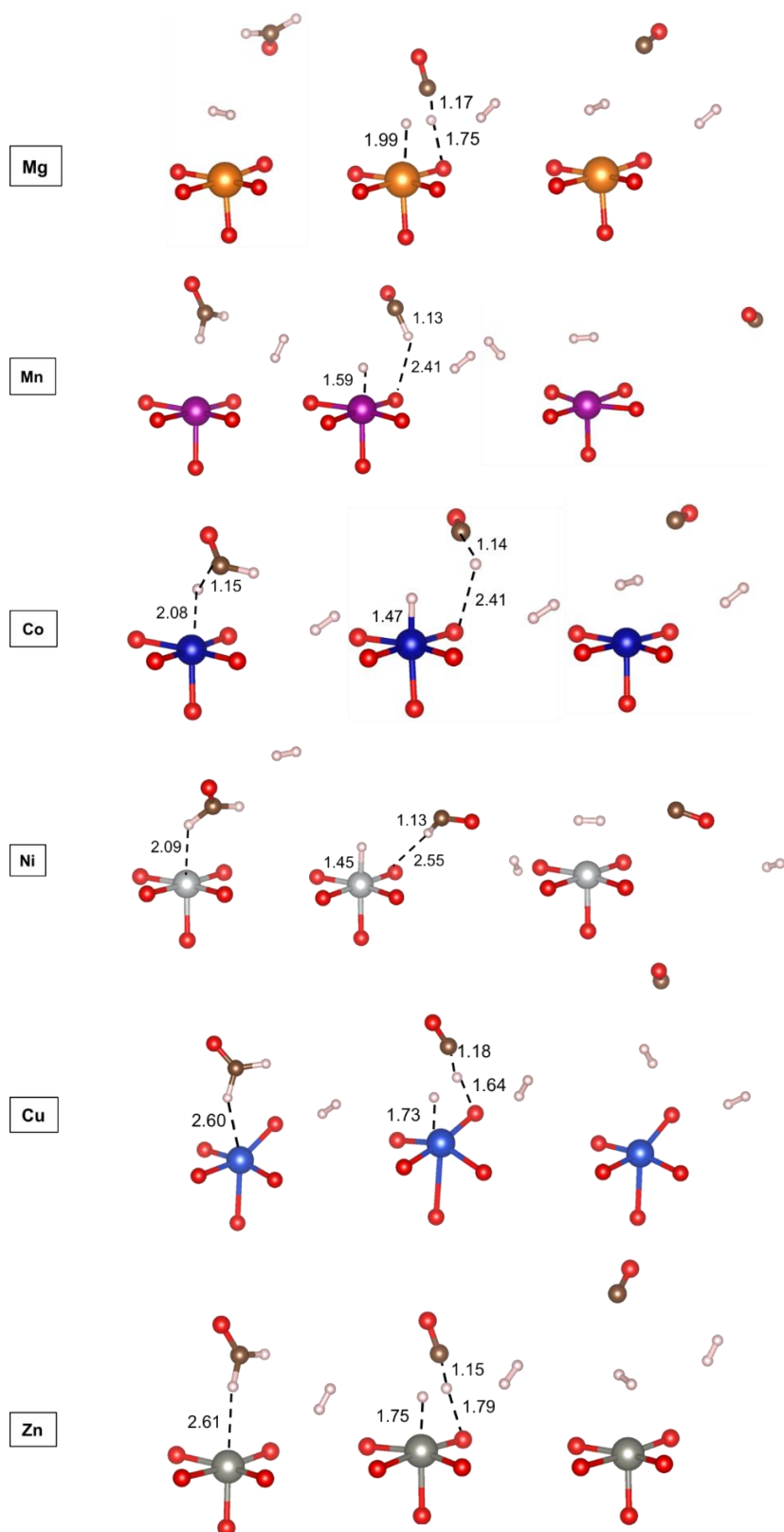


Figure S12. Geometry of the transition state structures and intermediates around it involved in (a) the dehydrogenation of methanol to formaldehyde and (b) the dehydrogenation of formaldehyde to carbon monoxide catalyzed by M-MOF-74 and assisted by the linker. Simplified models, with only the first coordination sphere of a single metal site depicted, are shown. The O atoms are bound to the linker molecules as shown in the full cluster model (Figure S11c). (Color coded such that O = red, C = brown, H = white, metal = others).

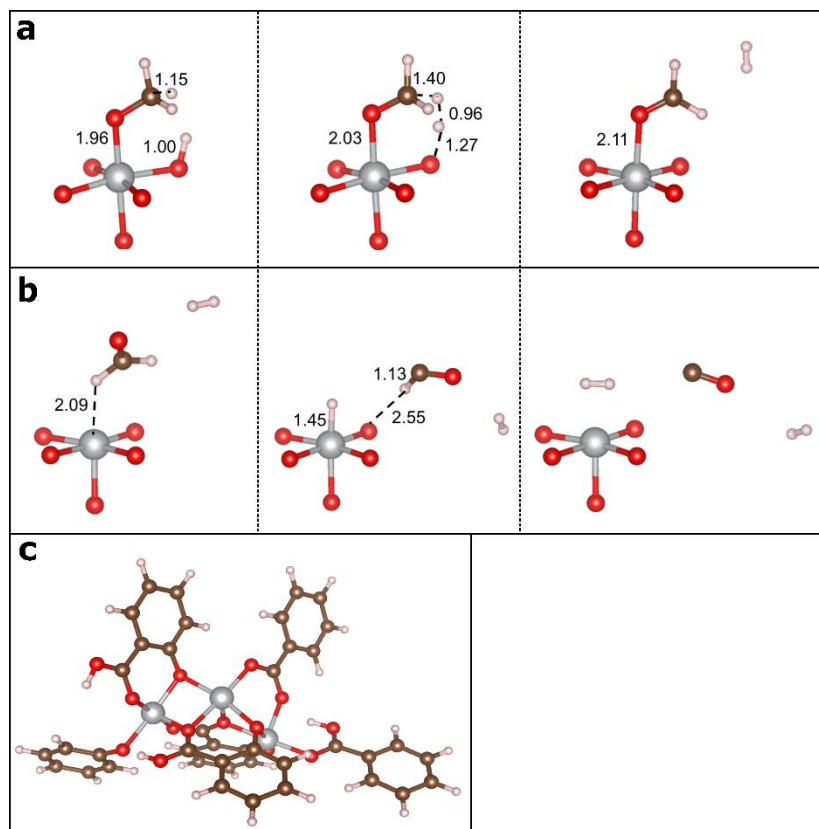


Figure S13. Geometries of the transition states (middle) and reaction species (left/right) involved in (a) the dehydrogenation of methanol to formaldehyde (Reaction 1) and (b) the dehydrogenation of formaldehyde to carbon monoxide (reaction 2) catalyzed by Ni-MOF-74 when assisted by the linker. Simplified models, showing only the first coordination sphere of a single metal site, are shown (Color coded such that Ni = gray, O = red, C = brown, and H = white). The oxygen atoms are bound to the linker molecules as shown in the full cluster model (c). The intermediates were determined by following the minimum energy path starting from the transition structure. Transition states for other M-MOF-74 structures can be found in Figure S12.

Table S7. Barrier heights (ΔH^\ddagger , kcal/mol)^a and reaction energies (ΔH , kcal/mol)^b of (1) the dehydrogenation of methanol to formaldehyde and (2) the dehydrogenation of formaldehyde to carbon monoxide for the reaction catalyzed by each M-MOF-74 and referenced against the uncatalyzed reaction. Lower barrier heights are observed when the reaction at the OMS is assisted by the linker, as shown in Figure S13. Enthalpies calculated by PBE/def2-TZVP using the cluster model.

Metal in M-MOF-74	Catalysis at unassisted OMS				Catalysis at OMS assisted by linker			
	ΔH^\ddagger_1	ΔH_1	ΔH^\ddagger_2	ΔH_2	ΔH^\ddagger_1	ΔH_1	ΔH^\ddagger_2	ΔH_2
Cu	72.4	23.4	73.0	10.2	9.8	-15.4	58.7	8.7
Co	70.0	22.2	78.9	15.9	8.9	-13.5	47.8	8.2
Mg	66.5	27.2	78.1	15.2	0.3	-23.5	58.2	8.4
Mn	75.3	25.6	78.7	15.9	3.4	-17.5	48.8	6.7
Ni	75.6	25.0	79.6	17.2	0.7	-20.8	47.0	7.6
Zn	75.4	22.9	77.7	12	2.3	-18.2	57.0	4.2
Uncatalyzed	79	21	74	7	-	-	-	-

^aThe barrier heights are calculated with respect to the immediate intermediate preceding the transition structure.

^bReactant adsorption and product desorption are not considered in the reaction energies. The reaction energies are calculated as the difference in energies between the product complex and the reactant complex.

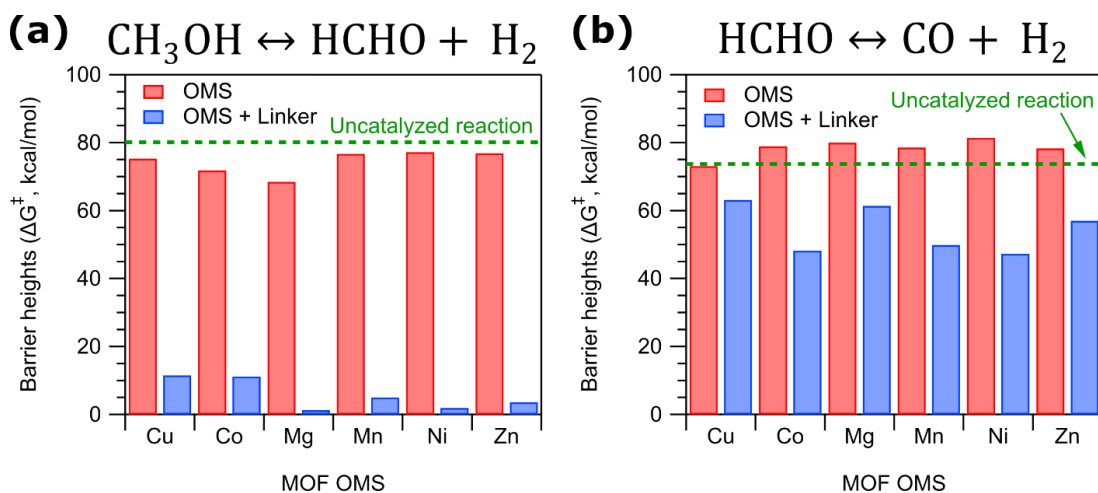


Figure S14. Visualization of the reduced barrier heights reported in Table 1 of the manuscript. The linker-assisted pathway has significantly reduced barriers for the two reaction steps.

Table S8. Lattice parameters and volumes of bimetallic MOF-74 structures calculated by systematically substituting the 6 atoms in the periodic model (Ni_0Mg_6 to Ni_6Mg_0) as shown in Figure S12. The energy of isocompositional structures is also shown, relative to Ni_2Mg_4_5 . The PBE functional is used for all the calculations.

Metal in M-MOF-74	Lattice parameter (\AA)			Volume (\AA^3)	Relative energy (kcal/mol)
Mg ₆	6.91	15.25	15.25	1361.3	-
Ni ₁ Mg ₅	6.88	15.42	14.87	1348.1	-
Ni ₂ Mg _{4_1}	6.86	15.02	15.07	1340.3	2.1
Ni ₂ Mg _{4_2}	6.86	15.05	15.53	1339.4	2.1
Ni ₂ Mg _{4_3}	6.85	15.06	15.56	1341.2	0.9
Ni ₂ Mg _{4_4}	6.85	15.03	15.07	1341.6	0.9
Ni ₂ Mg _{4_5}	6.85	14.39	15.50	1329.6	0.0
Ni ₆	6.77	15.01	14.98	1289.5	-

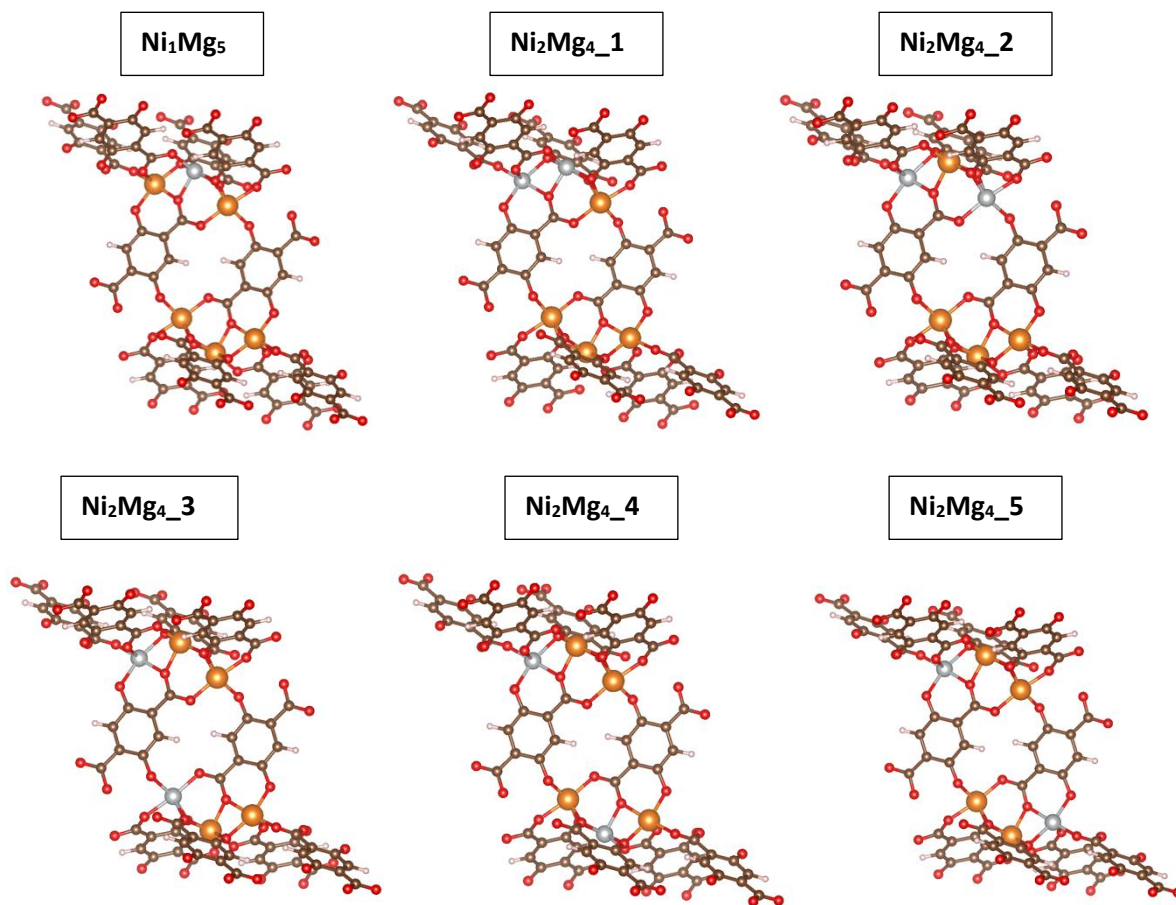


Figure S15. Six bimetallic $(\text{Ni}_x\text{Mg}_{6-x})$ -MOF-74 structures presented in Table S4. Colored such that Ni = gray, Mg = orange, O = red, C = gray, and H = pink.

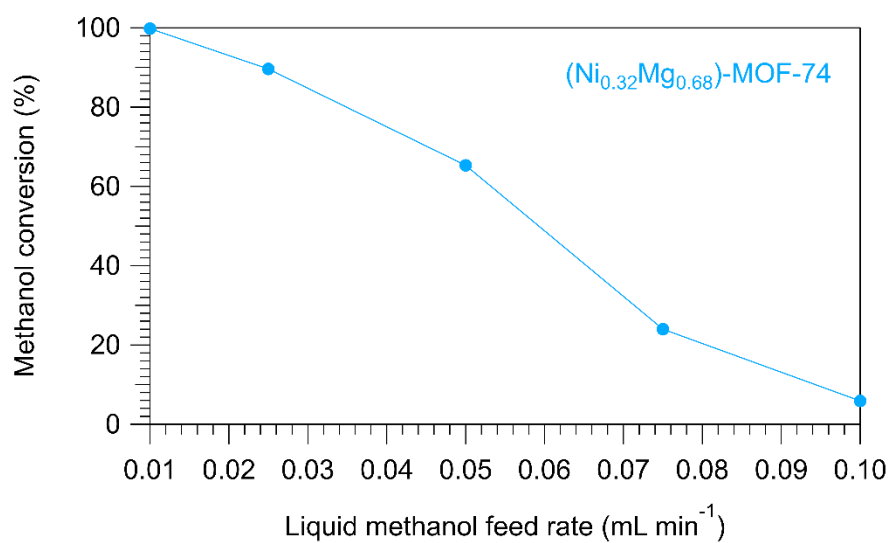


Figure S16. Effect of methanol feeding rate on methanol conversion with the $(\text{Ni}_{0.32}\text{Mg}_{0.68})$ -MOF-74 catalysts. Reaction condition: $35 \text{ ml N}_2 \text{ min}^{-1}$, 100 mg catalyst, $250 \text{ }^\circ\text{C}$ and 1 atm.

References

1. P. D. C. Dietzel, R. Blom and H. Fjellvåg, *Eur. J. Inorg. Chem.*, 2008, **2008**, 3624-3632.
2. J. Schwan, S. Ulrich, V. Batori, H. Ehrhardt and S. R. P. Silva, *Journal of Applied Physics*, 1996, **80**, 440-447.
3. P. D. C. Dietzel, B. Panella, M. Hirscher, R. Blom and H. Fjellvåg, *Chem. Commun.*, 2006, 959-961.
4. T. C. Wang, J. L. White, B. Bie, H. Deng, J. Edgington, J. D. Sugar, V. Stavila and M. D. Allendorf, *ChemPhysChem*, 2019, **20**, 1305-1310.
5. G. Calleja, R. Sanz, G. Orcajo, D. Briones, P. Leo and F. Martínez, *Catal. Today*, 2014, **227**, 130-137.
6. T. Grant Glover, G. W. Peterson, B. J. Schindler, D. Britt and O. Yaghi, *Chemical Engineering Science*, 2011, **66**, 163-170.
7. Z. Zhang, J. Su, A. S. Matias, M. Gordon, Y.-S. Liu, J. Guo, C. Song, C. Dun, D. Prendergast, G. A. Somorjai and J. J. Urban, *PNAS*, 2020, 29442-29452.
8. M. Mihaylov, T. Tsoncheva and K. Hadjiivanov, *J. Mater. Sci.*, 2011, **46**, 7144-7151.
9. Y. Usami, K. Kagawa, M. Kawazoe, Y. Matsumura, H. Sakurai and M. Haruta, *Appl. Catal. A*, 1998, **171**, 123-130.
10. L. N. Chen, K. P. Hou, Y. S. Liu, Z. Y. Qi, Q. Zheng, Y. H. Lu, J. Y. Chen, J. L. Chen, C. W. Pao, S. B. Wang, Y. B. Li, S. H. Xie, F. D. Liu, D. Prendergast, L. E. Klebanoff, V. Stavila, M. D. Allendorf, J. Guo, L. S. Zheng, J. Su and G. A. Somorjai, *J. Am. Chem. Soc.*, 2019, **141**, 17995-17999.
11. N. Takezawa and N. Iwasa, *Catal. Today*, 1997, **36**, 45-56.
12. T. Pham, K. A. Forrest, R. Banerjee, G. Orcajo, J. Eckert and B. Space, *J. Phys. Chem. C*, 2015, **119**, 1078-1090.
13. T. Pham, K. A. Forrest, J. Eckert and B. Space, *Cryst. Growth Des.*, 2016, **16**, 867-874.
14. L. Valenzano, B. Civalieri, S. Chavan, G. T. Palomino, C. O. Areán and S. Bordiga, *J. Phys. Chem. C*, 2010, **114**, 11185-11191.